AGU Monograph: ENSO in a Changing Climate

Chapter 13. ENSO Response to Greenhouse Forcing

Wenju Cai[1,2], Agus Santoso[2,3], Guojian Wang[1,2], Lixin Wu[1], Mat Collins[4], Matthieu Lengaigne[5], Scott Power[6], Axel Timmermann[7,8,9]

[1]Key Laboratory of Physical Oceanography/Institute for Advanced Ocean Studies, Ocean University of China and Qingdao National Laboratory for Marine Science and Technology, Qingdao, China.

[2]Centre for Southern Hemisphere Oceans Research (CSHOR), CSIRO Oceans and Atmosphere, Hobart, Tasmania, Australia

[3]Australian Research Council (ARC) Centre of Excellence for Climate Extremes and Climate Change Research Centre, The University of New South Wales, Sydney, NSW, Australia.

[4]College of Engineering, Mathematics, and Physical Sciences, University of Exeter, Exeter, UK

[5]LOCEAN/IPSL, Sorbonne Universités/UPMC-CNRS-IRD-MNHN, Paris, France

[6]Australian Bureau of Meteorology, Melbourne, Victoria, Australia

[7]Center for Climate Physics, Institute for Basic Science (IBS), Busan, South Korea

[8]Pusan National University, Busan, South Korea

[9]International Pacific Research Center, University of Hawaii at Manoa, Honolulu, HI, USA

Corresponding email: wenju.cai@csiro.au

Abstract

How ENSO responds to an increasing concentration of greenhouse gases in the atmosphere has remained an elusive issue for decades. Climate models produce widely diverging results based on the traditional sea surface temperature (SST) metrics of ENSO. Some models show stronger ENSO, some weaker, some show no clear change. Steering away from these static measures, but more carefully examining the underlying processes and the associated key physical characteristics of ENSO, a clearer picture begins to emerge. Due to the nonlinear response of the atmosphere to SSTs, an enhancement in ENSO-driven precipitation is favored. Such a response tends to be robust across models featuring relatively strong inter-model agreement in the projected changes of the Pacific mean climate, marked by equatorially enhanced warming and weakened Walker Circulation. These mean-state changes facilitate increased frequency of extreme El Niño events in models that are able to simulate nonlinear properties of ENSO closer to observations. In this ensemble of selected models, the frequency of extreme La Niña events is also projected to increase, as facilitated by faster warming of the Maritime Continent than the surrounding ocean waters. A projected increase in upper-ocean stratification further favors increased variability and occurrences of Eastern Pacific El Niño. Uncertainties however remain due to persistent model biases, highlighting the need to further improving climate models, as well as sustaining reliable observations to constrain model projections. Nonetheless, these projections underscore a possible heightened impact of ENSO-driven changes in a warming climate.

13.1. Introduction

Given the significant global-scale impact of ENSO on society, economy, and the environment, understanding how ENSO responds to greenhouse forcing is an urgent critical issue as global greenhouse-gas emissions continue unabated. While ENSO as a naturally occurring climate phenomenon will continue to operate in the warmer future, crucial questions remain which are of relevance to climate and disaster risk management. Will it change in character? Will it become more or less active, stronger or weaker? And if so, what are the mechanisms? Are the climate models used to make the projections reliable? This chapter discusses the current state of understanding that is relevant to addressing these questions, indicative to the possibility that ENSO will respond to future anthropogenic greenhouse forcing in some significant ways.

Considering the multitude delicate processes governing ENSO characteristics and evolution as described in earlier chapters of this book, it is not surprising that projecting future ENSO behavior is a challenging undertaking. Every element of the dynamical processes can respond directly to greenhouse forcing, or indirectly via changes in other components of the climate system. This complexity has also posed a great challenge in simulating a realistic ENSO in climate models that are used to make the projections (Chapter 9). ENSO is tightly linked to the tropical Pacific mean climate upon which it evolves (Chapter 8), so it is necessary to understand how the mean climate might change under greenhouse forcing. This will be first discussed in section 13.2. Section 13.3 explains the fundamental reasons for why at a first impression there was no agreement among climate models in the projected ENSO changes. It is not until recently that more robust projections started to emerge, owing to more careful considerations of the nonlinear nature of ENSO. This is to be covered in section 13.4 outlining the projected changes in atmosphere and oceanic aspects of ENSO dynamics along with the associated mechanisms. Section 13.5 discusses the uncertainties underlying the future projections tied to model biases. The chapter concludes in section 13.6 with a summary and concluding remarks.

13.2. Forced changes in background climate

Under ENSO neutral conditions, the tropical Pacific climate is characterized by the westward blowing Trade Winds that pile up warm waters in the Western Pacific. The Western Pacific warm pool exhibits annual mean SSTs above 28°C, a necessary condition for maintaining deep atmospheric convection above the ocean (Graham & Barnett, 1987). The warm pool hence hosts an almost permanent deep atmospheric convection, in which mid-tropospheric heating drives the ascending branch of the Walker Circulation and surface easterlies over the eastern and central equatorial Pacific. The rising air flows eastward in the upper troposphere and subsides over the relatively cold and dry eastern equatorial Pacific (see Fig. 1 in Chapter 1). The equatorial Trade Winds generate strong upwelling in the eastern equatorial Pacific through Ekman divergence. The easterly momentum transfer from the equatorial trades to the ocean is balanced by a zonal oceanic pressure gradient, which in turn causes the thermocline to shoal (deepen) in the eastern (western) tropical Pacific. The off-equatorial and equatorial trade winds also generate subtropical meridional oceanic circulation cells (McCreary & Lu, 1994), that transport the upwelled equatorial water poleward, while bringing back subducted subtropical waters towards the equator within the mean thermocline layer at about 100-200 m depths (e.g., Schott et al., 2004).

In response to increasing greenhouse gas emissions many climate models simulate a reduction of the eastern equatorial Pacific cold tongue and stronger warming along the equator than off-equator (Timmermann et al., 1999). This "enhanced equatorial warming" pattern (Liu, et al. 2005; Xie et al., 2010; Cai et al., 2015) is due to the fact that the evaporative damping of CO_2-induced warming is weaker in the equatorial strip compared to the off-equatorial regions, because the latent heat flux scales with the mean wind-speed, and the mean wind speed decreases towards the equator (Seager & Murtugudde, 1997; Xie et al., 2010). In addition to the characteristic meridional warming structure, most CMIP3 and CMIP5 models also simulate a slightly stronger warming in the eastern Pacific, compared to the west (e.g., Xie et al. 2010; Power et al., 2013). Climate models with a thermodynamic mixed-layer slab ocean can capture this response (e.g., Vecchi & Soden, 2007), sometimes even stronger than Coupled General Circulation Models (CGCMs).

Factors that may contribute to this zonally asymmetric response include a shallower mixed layer in the eastern Pacific, and asymmetric cloud feedbacks (stratus cloud feedback in the east, cumulus cloud/cirrus feedback in the west) (Meehl & Washington, 1996), but also a deepening of the eastern equatorial thermocline in response to weaker equatorial trade winds (see discussion below). However, the fact that some climate models (e.g., Kohyama et al., 2017) instead simulate a negative zonal SST gradient change along the equator in response to transient CO_2 radiative forcing, suggests that the upwelling of relatively cold water in the eastern Pacific and the associated thermodynamic damping ("dynamical thermostat"; Clement et al., 1996) can partly offset the CO_2-induced surface warming. This argument relies on the assumption that the older waters that upwell in the eastern equatorial Pacific had been exposed to lower atmospheric CO_2-induced warming the last time they were in contact with the surface. This non-equilibrium effect is likely to play an important role in transient climate change simulations, but not under equilibrated conditions in which the amount of warming at subsurface has caught up with that at the surface.

The enhanced eastern equatorial warming plays a key role in intensifying rainfall in the equatorial region over the 21st Century (e.g., Vecchi & Soden, 2007; Cai et al. 2014; Power and

Delage 2018), due to an increased low-level moisture convergence. Such pattern of rainfall changes is consistent with a 'warmer gets wetter' hypothesis (Xie et al., 2010) in which precipitation changes are closely tied to shifts in atmospheric circulation and moisture convergence (Chadwick et al., 2012; Widlansky et al., 2013).

The majority of climate models forced with increasing greenhouse gas concentrations show a slow-down of the Walker Circulation (Vecchi et al., 2007; Power & Kociuba, 2011a; Kociuba & Power 2015). Following the Clausius-Clapeyron relation (Clausius, 1850; Clapeyron, 1834), the saturated water vapor in the lower troposphere increases at a global mean rate of about 7% K^{-1} of global warming. Climate models support this thermo-dynamical relationship – at least on a global scale (Collins et al., 2010). However, the rate of precipitation increase is much lower (~2% K^{-1}). Because the precipitation increase does not keep up with the increase in humidity, there must be a reduction in the mass flux from the moist boundary layer into the dryer air aloft (Held & Soden, 2006). As a consequence, atmospheric vertical motion over tropical convective regions, such as the Western Pacific Warm Pool, is expected to decrease (~5-10% K^{-1}), leading to a slow-down in the atmospheric overturning circulation. Even though this argument links the thermodynamics of global warming with atmospheric dynamics, it does not entirely explain how the atmospheric circulation will slow down and whether the slow-down will affect the Walker and Hadley circulation cells. Other factors, such as the enhanced equatorial warming (e.g., Liu et al., 2005) and off-equatorial rainfall increase driven by the background sea surface warming (Kug et al., 2011), can further contribute to the Walker Circulation slow down. The wind change also leads to a reduction of Ekman divergence and equatorial upwelling (Vecchi & Soden, 2007; DiNezio et al., 2009; see Collins et al., 2010 and Cai et al., 2015 for a review). As a result, the east-west tilted thermocline flattens, which can further amplify the initial equatorial warming, in particular in the eastern equatorial Pacific.

Regarding the Hadley Circulation, the situation is more complex, because on top of an overall slow-down of the meridional mass stream function (e.g., Vecchi & Soden, 2007; Lu et al., 2007; Seo et al., 2014), there is also evidence for a "deep tropical squeeze" (Lau & Kim, 2015), which tends to enhance the near-equatorial circulation characteristics. Furthermore, given the Hadley cells are influenced by atmospheric stratification, meridional surface temperature gradients, and extratropical eddy dynamics (Schneider, 1977; Seo et al., 2014; Walker & Schneider, 2006), their future strength and properties can be influenced by changes in these various elements.

It should be noted here that even though the tropical Pacific warming pattern and an El Niño bear some similarities in terms of their surface temperature characteristics, the underlying processes responsible for the pattern formation are very different. The greenhouse gas-induced westerly wind anomalies cover the entire equatorial Pacific, whereas westerly wind anomalies during an El Niño are confined to the western to central part of the Pacific basin. The weaker Walker Circulation under global warming reduces poleward heat transport, which is near symmetrical about the equator (e.g., Liu et al., 2017). In contrast, there tends to be a net northward heat transport across the equator during an El Niño event (e.g., McGregor et al. 2014). The seasonality of the anomalous equatorial Pacific warming may also be different: For instance, in the GFDL CM2.1 model, during an El Niño it tends to peak toward boreal winter, whereas the greenhouse warming response peaks around mid-calendar year (Xie et al., 2010). Further, sea level pressure over tropical South Pacific decreases during an El Niño, but an increase may be detected under global warming (Xie et al., 2010) as would be reflected in the Southern Oscillation Index (SOI) which is negative during El Niño years, whereas under global warming the SOI increases (Power and Kociuba, 2011b). This contrast arises because the SOI depends on MSLP spatial differences, and MSLP changes over the Pacific under global warming and during El Niño years tend to have a different spatial structure (Power & Kociuba, 2011b).

While the projected mean-state changes outlined above tend to be consistent across models, confidence in these projections is reduced by the existence of observational uncertainty and model biases, and uncertainty in estimates of long-term climate trends derived from different observational datasets.

Disentangling long-term observed SST trends in the tropical Pacific in terms of externally forced signals and corresponding feedbacks and natural variability has been hampered by the fact that the different SST observational products show opposing patterns, in particular in the eastern equatorial Pacific (Vecchi et al., 2007; Deser et al., 2010; An et al., 2012). A multivariate statistical decomposition which includes a removal of ENSO, suggests a more robust strengthening of the prevailing SST gradients (Solomon & Newman, 2012) over the period from 1900-2010 – the extent of which is not captured by CMIP5 models (Coats & Karnauskas, 2017). This result would support the role of the "ocean dynamical thermostat" (Clement et al., 1996, Cane et al., 1997), particularly during the boreal fall when the climatological SST gradient is the strongest (Karnauskas et al., 2009). This strengthening of the east-west SST gradient occurs despite a weakening of sea level pressure gradient which indicates a weakened Walker Circulation and Trade Winds (Karnauskas et al., 2009). This near centennial trend could suggest a greenhouse forcing effect that may manifest in stronger zonal SST gradients, although uncertainties still exist in the observational data prior to 1950 (see Chapter 3) and due to the fact that the greenhouse warming signal, natural interdecadal variability and ENSO share some pattern characteristics. In addition, these patterns may also vary over a shorter period. Over 1950-2009, for instance, the zonal SST gradient was found to weaken (Tokinaga et al., 2012a), consistent with the weaker winds (Tokinaga et al., 2012b). However, these are inconsistent with analysis of sea level pressure based on several observational products which instead suggested a stronger Walker Circulation (L'Heureux et al., 2013). These inconsistent changes between zonal SST gradient and Walker Circulation again differ from the case of El Niño in which weaker east-west SST gradient associated with warmer eastern equatorial Pacific is accompanied by weaker Trade Winds through the Bjerknes feedback – a positive feedback loop that sustains ENSO event development (Chapters 1, 2). Under greenhouse warming though, stronger zonal SST gradient may not necessarily be accompanied by stronger Walker Circulation (An, 2011).

Diagnosing greenhouse effect in the relatively short observational record is complicated by naturally occurring decadal variability, such as the Interdecadal Pacific Oscillation (IPO; Power et al. 1999). Shifts in the Pacific climate associated with the IPO were observed in the mid 70's from a negative IPO to a positive IPO, followed by a shift to a negative in the late 90's. The positive IPO phase was characterized by an SST trend, with stronger warming east of the Dateline and weaker Trade Winds (e.g., Meehl & Washington, 1996). The latter was marked by unprecedented acceleration of the Walker Circulation (Kociuba and Power, 2015), along with a cooler tropical Pacific that contributed to the global warming hiatus (Kosaka and Xie, 2013, England et al. 2014). Correspondingly, there were marked changes in ENSO properties. The positive IPO state saw stronger ENSO variability in the eastern equatorial Pacific marked by the 1982/83 and 1997/98 extreme El Niño events, and the negative IPO state had stronger variability in the central Pacific (e.g., Wang and An, 2001; Lee & McPhaden, 2012; Santoso et al. 2017). The link between IPO and ENSO variability is still a topic of intense research, which is further complicated by the fact that mean state changes can influence ENSO properties (e.g., Fedorov & Philander, 2000; Wang and An, 2002; Power et al. 2013), while changes in ENSO variability can in turn influence multi-decadal variability (Timmermann, 2003; Rodgers et al., 2004; Power & Colman, 2006; Sun et al., 2014; Newman et al., 2016).

It is necessary to stress that climate models still suffer from persistent biases (oftentimes larger than their projected global warming responses), thus leaving uncertainties in the projected mean-state changes despite the reasonably strong inter-model consensus on the projections. A well-known model deficiency is the Pacific "cold tongue" bias in which the ribbon of cool eastern equatorial Pacific water extends too far west into the Western Pacific Warm Pool, with the stronger than observed Trade Winds, and a double Intertropical Convergence Zone bias (Chapter 9). It is not entirely clear what ramifications such biases have on future projections, but recent research (Li et al., 2016; Ying et al., 2018) indicates that models with less severe cold-tongue bias tend to project a warming pattern with stronger SST warming in the east Pacific (see Section 13.5 for a discussion).

13.3. Elusive projections of ENSO

Despite relative inter-model agreement on the projected change in the 21st Century mean climate, there is a lack of consensus on the change in ENSO as typically diagnosed in terms of SST variability at fixed locations in the equatorial Pacific, such as in the Niño3, Niño3.4, and Niño4 regions. SST is a core variable for ENSO as it is the main way through which ocean-atmosphere feedbacks are mediated, thus the Niño indices have been widely used across research and prediction platforms to characterize and monitor ENSO events.

Investigations of how ENSO SST variability could change in response to global warming started in the '90s, using climate models that were considered advanced at the time. These studies found little or no changes in future ENSO behavior (e.g., Meehl et al., 1993; Tett, 1995; Knutson et al., 1997). However, the reliability of the results was questionable given the models deficiencies in simulating the complex interacting processes involved in ENSO. Using a model with a more realistic representation of ENSO in part due to higher resolution that can better resolve equatorial wave dynamics, Timmermann et al. (1999) found more frequent El Niños and stronger cold events in the eastern equatorial Pacific under a future emission scenario. The authors argued that a long-term increase of vertical stratification in the eastern tropical Pacific enhanced the sensitivity of SST to ENSO-related wind stress forcing. This higher sensitivity would strengthen the thermocline feedback and may thus contribute to ENSO amplitude changes. A follow-up study (Timmermann, 2001) then presented evidence for a major change of ENSO stability during this greenhouse warming simulation, which translated into rapid amplitude shifts. Stronger and more frequent ENSO were also found in another model, the Hadley Centre coupled model version 2 (HadCM2), under a four-time pre-industrial CO_2 levels (Collins, 2000a). In stark contrast, in spite of being forced with the same greenhouse gas concentration, no appreciable response was found in the third version of the Hadley Centre model (HadCM3) which had enhanced horizontal ocean resolution, exclusion of flux adjustments, and subtle changes in the sub-grid scale parameterization schemes that can affect cloud formation (Collins, 2000b). This discrepancy is an early example of model-based uncertainties in ENSO projections.

Since the '90s, the performance of climate models in simulating ENSO has notably improved, despite stubborn common biases (see Chapter 9). Facilitated through CMIP, an increasing body of studies have now analyzed ensembles of different climate models, run with the same forcing under equivalent emission scenarios. Results from the third phase of CMIP (CMIP3) still showed no inter-model consensus in terms of amplitude and frequency of ENSO SST variability (van Oldenborgh et al., 2005; Merryfield, 2006; Guilyardi, 2006; Yeh & Kirtman, 2007; Latif & Keenlyside, 2009; Collins et al., 2010), nor did models that participated in the later inter-comparison project (CMIP5) (Stevenson, 2012; Santoso et al., 2013; Bellenger et al., 2014; Taschetto et al., 2014; Kim et al., 2014; Cai et al., 2015; Chen et al., 2017). Some models showed an increase in the amplitude of ENSO SST variability, some a decrease, and some showed no appreciable change.

One reason for the variety of responses can be explained by the fact that ENSO SST variability essentially arises from an imbalance between positive and negative feedback processes. For instance, during the growth phase of an El Niño, positive feedback processes dominate the negative ones (Stein et al., 2010), resulting in a positive temperature tendency or heating rate (T_t). If the negative feedback processes dominate, then T_t is negative, resulting in a cooling of the mixed layer. This can be expressed mathematically in terms of a mixed-layer heat budget, which decomposes the rate of change of potential temperature *T* into the different contributing terms:

$$\int_{-H_m}^{0} T_t\, dz = \int_{-H_m}^{0} \left\{ Q' - \left[\left(u'T'_x + \bar{u}\, T'_x + u'\bar{T}_x\right) + \left(v'T'_y + \bar{v}\, T'_y + v'\bar{T}_y\right) + \left(w'T'_z + \bar{w}T'_z + w'\bar{T}_z\right) \right] \right\} dz + Res \quad , \qquad (1)$$

where Q is the net balance between shortwave and long-wave radiations, and latent-heat and sensible heat fluxes at the air-sea interface [divided by the product of a reference density of

~1026 kg m^{-3}, specific heat capacity of seawater (3986 J kg^{-1} K^{-1}), and mixed layer depth (~50 m]. The ocean current variables, u, v, and w, denote currents in the zonal, meridional, and vertical direction. The subscripts x, y, z are spatial derivatives in the zonal, meridional, and vertical direction, respectively, and prime indicates deviation from the climatological state denoted by the overbar. These collective terms are integrated across the surface mixed layer of depth H_m (50 m is a reasonable estimate for the average mixed layer depth in the equatorial Pacific), and the residual term, *Res*, contains unresolved processes such as mixing and diffusion.

The main positive feedback processes for ENSO are contained in the square bracketed terms in Eq. (1) of which the current and temperature anomalies are linked to anomalous winds and thermocline. The zonal advective feedback is contained in the $-u'\overline{T}_x$ term, where anomalous zonal current acts on the zonal gradient of the climatological mixed-layer temperature. During a developing El Niño, this term is positive (anomalous eastward advection of warmer western tropical Pacific waters), as the climatological zonal temperature gradient is negative (cooler temperature in the eastern Pacific than in the west) and u' is positive due to westerly wind anomaly and deeper thermocline along equator than off-equator, following the Ekman and geostrophic relations (see Chapter 6). The Ekman pumping feedback is associated with the $-w'\overline{T}_z$ term, which is also positive during an El Niño, since weaker zonal winds lead to weaker upwelling (i.e., $w' < 0$) and $\overline{T}_z$ is positive as climatologically the surface water is warmer than subsurface. The thermocline feedback is associated with the $-\overline{w}T_z'$, which is again positive during an El Niño development, as warm anomalies are stronger in the subsurface than at the sea surface (i.e., $T_z' < 0$) and the climatological vertical velocity anomaly is upward positive for upwelling. Q' is typically a negative feedback or damping term for ENSO SST anomalies: warmer sea surface produces more cloud that reduces incoming solar radiation and enhances latent heat, together acting to cool the surface waters. The opposite generally applies for La Niña, although significant asymmetries exist (Chapter 4), originating from the non-linear terms in Eq. (1).

Thus, the heating rate of the east Pacific mixed layer and sea surface temperatures is a net result of a delicate balance across several various positive and negative feedback processes. Because both the positive and negative feedback processes are, in general, projected to increase under global warming (e.g., Philip & van Oldenborgh, 2006; Kim et al., 2011), it may not be very surprising to find diverse changes in ENSO variability across models. Also notice that these feedback processes are a function of the mean basic states, as illustrated in Eq. (1) (see also

Chapters 6-8). Thus, changes in the mean state described in section 13.2 affect ENSO projections. Most climate models simulate stronger sensitivity between the wind forcing and ocean dynamical response (i.e., currents and thermocline) over the 21st Century (e.g., Kim et al., 2011; Chen et al., 2017). This is likely due to increased upper-ocean stratification associated with surface intensified warming and thinner mixed layer due to weaker winds, thus bringing the thermocline closer to the surface. Along with the consistent mean-state changes across models, the increased sensitivities tend to enhance the positive feedbacks across models. At the same time, the negative feedback of air-sea thermodynamic damping (i.e., sensitivity between sea surface temperature and net air-sea heat flux, Q) is also projected to enhance across models, due to climatologically increased evaporation and cloudiness (Knutson and Manabe 1995).

The results discussed above are generally based on ensembles of any available models without scrutinizing their performance in simulating the relevant processes. More recently, performing model selection based on the fidelity in simulating certain aspects of the observed ENSO (e.g., van Oldenborgh et al., 2005) has become common practice. In many cases, such approach has led to statistically significant detectable changes. For example, when examining only models that most realistically simulate the aforementioned linear feedback processes (Jin et al., 2006), Kim et al. (2014) found an inter-model consensus in the ENSO SST amplitude response that is time varying. In these “more realistic” models, the ENSO amplitude strengthens before 2040 when the eastern Pacific warms faster than the maritime region, before decreasing thereafter when the maritime region warming catches up, although the reason for this behavior is not entirely clear. On the other hand, the excluded models exhibit a persistent ENSO amplitude increase in the ensemble mean, but with large inconsistency in the trend across the models. It turned out that the excluded models tend to exhibit stronger cold tongue bias, thus potentially indicating that model bias may affect uncertainty in ENSO projections. In addition, the time-varying nature of the response itself also contributes to weaker inter-model consensus when examining changes averaged across the entire 21st Century.

Despite the elusive projections of ENSO SST variability at fixed locations discussed above, there is relatively strong inter-model agreement on how global warming will impact ENSO-driven precipitation in the tropical Pacific (Power et al., 2013). This will be reviewed in the next section, along with how consideration of atmospheric and non-linear processes, as well as application of model selection can lead to further insights about how ENSO behavior will change in the future.

13.4. Process-based ENSO projections

Even though the conventional SST metrics for ENSO do not provide a clear consensus picture of how ENSO amplitude will respond to greenhouse warming (Section 13.3), it does not necessarily imply there are no robust changes in the behavior and characteristics of ENSO. There are a number of atmosphere and oceanic processes involved in setting the spatial and temporal evolution of ENSO. These specific underlying processes, which are to a large extent nonlinear and linked to the mean state, could respond to and in turn contribute to climate change, potentially affecting some aspects of ENSO in a robust and significant way. Thus, to better understand how greenhouse warming would affect ENSO, it is important to look closely into each of these processes. This section illustrates that robust changes in ENSO could manifest in terms of the frequency of ENSO extremes arising from the interaction between the mean state and nonlinear processes. The non-linear processes are not well captured by every model which is in part why the multi-model picture does not tell the whole story.

13.4.1 ENSO-driven precipitation response

We first begin the discussion by stressing the results that the nonlinear atmospheric response to ENSO-driven SST variability in a warming world gives rise to greater agreement among models on changes in ENSO-driven precipitation variability under various warming scenarios, than they do for changes in ENSO-driven SST variability (Cai et al. 2012; Power et al., 2013; Watanabe et al., 2014; Cai et al., 2014; Chung and Power, 2014; Chung et al., 2014; Huang & Xie, 2015; Huang, 2016). This is primarily due to two factors. Firstly, the atmospheric response to SST anomalies in the equatorial Pacific is nonlinear (e.g. Hoerling et al., 1997; Kang & Kug, 2002; Philip & van Oldenborgh, 2009; Dommenget, et al. 2013; Power et al. 2013; Chung et al., 2014; Takahashi & Dewitte, 2016). Secondly, there is a degree of inter-model agreement in the mean-state change (Section 13.2).

The tropical Pacific is characterized by surface waters warmer than 27.5°C west of the dateline toward the maritime continent, and along the major rainfall bands, the ITCZ and SPCZ. Elsewhere, the surface temperature gradually drops to about 20°C toward the coastal regions of the eastern equatorial Pacific. In this “cold tongue” region, atmospheric deep convection is inhibited, and strong positive SST anomalies such as those that occur during an extreme El Niño are required to elevate SSTs and weaken lateral SST gradients to trigger deep convection and thus intense precipitation in the eastern equatorial Pacific. This anomalous convection tends to occur on the western flank of the core SST anomalies, given that SSTs are warmer toward the maritime continent. On the other hand, the impact of negative SST anomalies during a La Niña on eastern equatorial Pacific rainfall is considerably weaker since the cold-tongue region is already cold, and so atmospheric convection cannot decrease any further. However, with increasingly strong cold anomalies, the atmospheric response to La Niña SST anomalies can be large in regions where SSTs are climatologically high, leading to poleward displacement of the ITCZ and SPCZ, and westward shift of maximum equatorial rainfall in the western Pacific warm pool (Chung et al., 2014).

The nonlinear interaction between background warming and ENSO-related SST anomalies could hence increase the rainfall response to ENSO SST (Power et al. 2013; Chung et al. 2014; Huang & Xie 2015; Huang, 2016). As the eastern equatorial Pacific is projected to warm in the future (according to multi-model ensemble mean projections), convection can indeed be more easily triggered, even for moderate El Niño events, thereby increasing rainfall considerably in response to a given El Niño SST anomaly (Cai et al., 2012; 2014). But this is achieved through severe weakening of zonal and meridional background SST gradients (Cai et al. 2012; 2014), rather than by simply exceeding the convective SST threshold since the threshold itself also increases in a warmer climate (Johnson & Xie, 2010) due to changing atmospheric background stratification. This spatial pattern of changes in background SST also shift the response pattern of rainfall eastward to the equatorial eastern Pacific and equatorward (Kug et al., 2011; Power et al. 2013; Cai et al., 2012; 2014; Zhou et al. 2014; Huang 2016), leading to more frequent swings of the SPCZ and ITCZ toward the equator (Cai et al., 2012; 2014), and the ENSO-related rainfall asymmetry is enhanced in some locations (Huang & Chen, 2017; Bonfils et al., 2015; Power & Delage, 2017). In essence, the reasons behind the robust projection of ENSO-related precipitation are atmospheric nonlinearity and inter-model agreement in the mean-state change, despite the uncertainty in future ENSO amplitude change (Power et al., 2013; Watanabe et al., 2014).

The nonlinear atmospheric response means that heavy rainfall can occur in the usually dry and cold eastern equatorial Pacific when SSTs in the region increase to significantly weaken or even reverse the otherwise positive meridional SST gradient. This occurs during an extreme El Niño when averaged boreal winter rainfall over the Niño3 region (5°S-5°N, 150°W-90°W) reaches more than 5 mm day^{-1}, as observed during the 1982/83, 1997/98, and 2015/16 extreme El Niño events (Fig. 13.3a). However, such a nonlinear feature that characterizes an extreme El Niño is not captured by all climate models (Cai et al., 2014), because of severity of the cold-tongue bias and the ability of models in simulating convection and cloud processes in the eastern equatorial Pacific (see Section 13.5 for discussions). Considering only models in the CMIP3 and CMIP5 archives that are able to simulate this atmospheric nonlinearity, Cai et al. (2014) found a doubling in the frequency of future El Niño events, as characterized by their atmospheric rainfall response, under a "business-as-usual" emission scenario (Fig. 13.3c, d). The frequency increase is not simply due to increased climatological rainfall in the cold-tongue region, but to increased likelihood of convective activity, as also indicated by increases in atmospheric vertical velocity (Cai et al., 2017), linked to changes in the mean state discussed above. From the perspective of rainfall impact, this indicates an increased frequency of extreme El Niño events under greenhouse warming.

13.4.2 Nonlinearity in oceanic variables

Robust future ENSO changes are not limited to the atmosphere, but are also found in the ocean. The weakened Walker Circulation associated with the eastern Pacific warming, leads to weaker equatorial Pacific currents (Vecchi & Soden, 2017), which can influence the evolution of ENSO SST anomalies through heat advection. An asymmetric propagation feature in ENSO SST anomalies along the equatorial Pacific puzzled researchers for decades (Wallace et al., 1998; Neelin et al., 1998; An and Jin, 2004). Specifically, why do SST anomalies appear to propagate westward during La Niña and moderate El Niño events, but eastward during an extreme El Niño of 1982/83 and 1997/98 (McPhaden & Zhang, 2009)? Linear theories showed that eastward propagation arises if the thermocline feedback dominates over other positive feedback processes, otherwise a westward propagation would result (Jin & Neelin, 1993). This would apply to both El Niño and La Niña, in stark contrast to the observed asymmetry. The effect of the positive feedback processes on zonal propagation was confirmed through a mixed layer heat budget analysis (Santoso et al., 2013). However this occurs amidst the interplay between nonlinear zonal advection ($-u'T'_x$) and the advection by the mean current ($-\bar{u}T'_x$) that was found to be a key factor in giving rise to the El Niño-La Niña propagation asymmetry in observations and models that are able to simulate this propagation asymmetry (Santoso et al., 2013). In essence, the strong eastward current anomaly during strong El Niño events is sufficiently large to overcome the westward mean current, such that the total current is eastward ($u' + \bar{u} > 0$), thereby advecting heat anomaly to the east. In all other cases (La Niña and moderate El Niño) the total current remains westward. Thus, as the mean current is projected to weaken under global warming, it would be easier for the current to reverse eastward during an El Niño. This leads to increased frequency of future eastward propagating El Niño events (Santoso et al., 2013). It should be noted that not all simulated extreme El Niño events identified based on the Niño3 rainfall threshold exhibit eastward propagation feature, but the converse is true (Cai et al., 2015b). In a similar token, the 2015/16 extreme El Niño exhibited large Niño3 rainfall, but did not exhibit a clear eastward propagation (Fig. 13.3a) due to the weak eastward current reversal (Santoso et al., 2017).

Aside from the projected faster warming of the eastern equatorial Pacific than the surrounding waters, the maritime continent is also projected to warm at a considerably faster rate than the surrounding waters (Cai et al., 2015). This leaves the equatorial central Pacific (Niño4 region; 5°S-5°N, 160°E-150°W) to be relatively cooler, thus increasing the likelihood for atmospheric subsidence and anomalously strong easterly winds to occur, which are conducive for strong La Niña events. In contrast to strong El Niño events which tend to have SST anomalies peaking in the eastern equatorial Pacific, strong La Niña events tend to peak in the central Pacific (e.g., Takahashi et al., 2011; Dommenget et al., 2013). Strongly negative Niño4 index distinguishes extreme La Niña events from moderate events (Fig. 13.3.b; Cai et al. 2015). As a salient feature of ENSO asymmetry (see Chapter 4), significant El Niño events tend to be followed by a La Niña, rather than the other way around – associated with El Niño-induced strong warm water volume discharge. The 1998/99 and 1988/1989 extreme La Niña events followed significant El Niño events in the previous year which left the equatorial Pacific subsurface cooler than normal (see Chapter 6). As a result, the thermocline shoals across the equatorial Pacific, promoting surface cooling that can initiate the Bjerknes feedback through Ekman pumping ($-w'\bar{T}_z$) involving easterly wind anomaly. The easterly wind anomaly promotes warming in the western Pacific, and this enhances zonal gradient of the anomalous surface temperature between the central Pacific and maritime continent, thereby further enhancing the Bjerknes feedback through nonlinear zonal advection ($-u'T'_x$). Under climate change, the faster warming of the Maritime Continent facilitates stronger nonlinear zonal advection, and the surface intensified warming favors the Ekman pumping feedback. In an ensemble of models that are able to simulate extreme El Niño (Cai et al., 2014), these favorable conditions for anomalous central Pacific cooling were found to support a near doubling in future occurrences of extreme La Niña events (Cai et al., 2015). The majority of the increase was found to be due to more frequent extreme El Niño events, thus depicting a future scenario of more extreme swings from an extreme El Niño to an extreme La Niña the following year (Fig. 13.3.c, d; Cai et al., 2015).

13.4.3 SST-based metrics revisited

The finding of increased frequency of ENSO extremes, which are inherently nonlinear, stresses the importance of considering nonlinear processes in understanding the effect of greenhouse warming on ENSO. While linear theories (e.g. the recharge oscillator) can explain much of ENSO evolution (Chapter 6), there is a substantial degree of nonlinearity in its basic spatial and temporal properties (Timmermann et al., 2018). The tendency for extreme El Niño anomalies to peak in the eastern equatorial Pacific, and extreme La Niña to peak in the western-central Pacific, results in a positively skewed SST anomaly in the Niño3 region and negative skewness in Niño4 region (Timmermann, 1999). These tendencies can be illustrated by decomposing the tropical SST anomaly into the first and second principal components (PC1 and PC2) via an empirical orthogonal function technique. The spatial pattern associated with PC1 represents the canonical El Niño with warm SST anomaly covering the eastern equatorial Pacific; whilst the second mode captures weaker positive SST anomaly straddling the central equatorial Pacific with a negative anomaly off the coast of Peru (see Fig. 3 of Takahashi et al., 11). Plotting PC1 against PC2, which respectively correspond to the Niño3 and the Trans-Niño indices (e.g., Santoso et al., 2017), results in an inverted 'V-shape" (Fig. 13.4a), underscoring the nonlinearity in ENSO patterns and magnitude. The combination between the two principal components depicts an ENSO diversity which encapsulates the tendency for strong El Niño events to peak in the eastern Pacific, and for moderate El Niño and strong La Niña events to peak in the central Pacific (Takahashi et al., 2011; Dommenget et al., 2013; Capotondi et al., 2015; see also Fig. 3a,b in Chapter 4). While the quasi-continuous distribution of SST anomalies in the PC1-PC2 space means that an ENSO event can peak anywhere across the equatorial Pacific, it also reveals two regimes of Eastern Pacific (EP) El Niño and Central Pacific (CP) El Niño, the former of which tends to be a stronger event (see Chapter 4).

Yeh et al. (2009) found that the frequency of CP El Niño would be greater than that of EP El Niño under greenhouse warming based on the premise that the weakened Trade winds would shoal the thermocline in the central Pacific which would in turn promote SST variability there. On the other hand, the reduced wind-driven upwelling should weaken the thermocline feedback, which governs EP El Niño. The result was based on a small sample of CMIP3 models that simulate the relative frequency of EP and CP El Niño closest to observations. There is no robust change in a larger sample of CMIP5 models (Taschetto et al., 2014), and the observed relative frequency itself can be affected by internal variability (Yeh et al., 2011). However, Power et al. (2013) showed that while CMIP5 models do a poor job in simulating the spatial pattern of CP El Niños, the four models best able to simulate them tend to exhibit an increase in the frequency of CP El Niños in response to global warming under RCP8.5. Nevertheless, the fact the SST biases are still larger than the SST amplitude of a typical CP ENSO event, suggests only low confidence in these results.

The degree of the nonlinear relationship between PC1 and PC2 can be quantified by fitting a quadratic function in the PC1-PC2 space: $PC2(t) = \alpha[PC1(t)]2 + \beta PC1(t) + \gamma$. Not all climate models can simulate the observed nonlinearity α, or equivalently the degree of ENSO diversity as seen in observations (Ham & Kug, 2012; Karamperidou et al., 2017). Models that capture the degree of observed α parameter tend to simulate a more realistic amplitude of the Bjerknes feedback components and shortwave damping in the eastern Pacific (Karamperidou et al., 2017), and these correspond to projection of eastern Pacific enhanced warming. The more realistic models should also be able to simulate shifts in atmospheric convection following the peak of El Niño warm surface anomaly, from the western to eastern Pacific as compared to the less realistic models which have convection more statically confined in the west due to the more severe cold-tongue bias (Ham & Kug, 2012). Examining CMIP5 models that have more realistic α parameter, Cai et al. (2018) showed that models with greater amplitude of α simulate greater amplitude of positive skewness in the Eastern Pacific and negative skewness in the Central Pacific, i.e., better simulating the nonlinear processes responsible for the skewness. Further, models producing greater amplitude of α simulate more distinct centres of CP and EP ENSO.

The core of SST anomalies associated with EP ENSO varies in location across the models, especially when the excluded models (based on the fidelity of the α parameter; Fig. 13.4d) are included in the ensemble. This reduces the robustness of projected ENSO amplitude when considering SST variability averaged over a region that is fixed across models (e.g., Niño3 index; see section 13.3). Using models that produce the two distinct anomaly centres, Cai et al. (2018) found a statistically 15% increase in SST variability associated with EP ENSO under greenhouse warming scenario (Fig. 13.4b, c, e). The enhanced variability translates to about 45% increase in the occurrences of strong EP El Niño. The cause for the increase is attributed to greenhouse gas-induced increased vertical stratification that enhances the coupling between wind and ocean which supports the Bjerknes feedback, as originally proposed by Timmermann et al. (1999).

13.5 Uncertainties and model biases

Errors and biases in models can influence the characteristics of the modelled ENSO and its projected response under climate change. Most CMIP models simulate an excessive westward extension of cold tongue and insufficient equatorial western Pacific precipitation (e.g. Mechoso et al., 1995; Li et al., 2015), which translates into an unrealistic extension of ENSO-related SST anomalies to the tropical western Pacific and westward shift of ENSO-related zonal wind stress and rainfall variability (Ham & Kug, 2014; 2015). In addition, most models still struggle to accurately represent feedback processes that control ENSO evolution. This includes a weaker than observed thermo-dynamical damping (e.g. Bellenger et al., 2014) as well as an underestimated positive ENSO feedbacks, which can also somewhat be connected to these aforementioned Pacific mean-state biases (e.g. Kim et al., 2014b). These compensating errors may still lead to realistic ENSO characteristics but with incorrect underlying ENSO dynamics (Bayr et al., 2018) and unrealistic sensitivities with respect to radiative perturbations. This fact may partly explain the diverse changes in ENSO SST variability across models (Kim et al., 2014b).

Several studies have attempted to identify sources of inter-model uncertainty in ENSO amplitude change, which appear to be linked with uncertainty in the climatological mean state. This can be done by examining inter-model relationship between changes in ENSO and various ocean-atmosphere parameters (e.g., Ham & Kug, 2016; Rashid et al., 2016; Chen et al., 2017). Some of the findings include a link between ENSO amplitude change with the climatological location of the convergence zones in present-day simulation, which controls the air-sea coupling strength change and the amplitude of ENSO variability (Ham & Kug, 2016). Chen et al. (2017) found that the CMIP5 inter-model divergence in the ENSO amplitude change is closely tied to the spread in the thermocline feedback changes which are in turn linked to changes in the mean equatorial upwelling and thermocline. Further, there is a statistically significant inter-model correlation between the change in ENSO amplitude and the relative SST warming pattern: models that project stronger ENSO amplitude tend to project stronger warming in the eastern Pacific (Zheng et al., 2016). Based on this inter-model relationship and to the extent that correcting present-day climatological biases, at least in a statistical sense, favours an eastern Pacific enhanced warming (Li et al., 2016; Ying et al., 2018), an increase in ENSO-related SST variance was likely under global warming (Zheng et al., 2016). This appears to support the overarching conclusion of more extreme ENSO events presented in section 13.4 based on an ensemble of selected models. There are however several other factors that remain to be investigated, which may affect such statistic-based corrections. For instance, Kohyama et al. (2018) suggested, based on a comparison of two climate models, that the more diffused thermocline in models compared to observations may instead render a weaker ENSO amplitude under greenhouse warming.

Several strategies have been proposed to alleviate the influence of model errors and biases on tropical Pacific future projections. A simple way is to perform a selection of models based on their ability to best simulate ENSO dynamics and characteristics (section 13.4). Another way is to dynamically correct the present-day model mean state. For instance, the impact of present-day CMIP biases on rainfall projections can be reduced by forcing an atmosphere-only model with bias-corrected SSTs (e.g. Knutson et al., 2008), i.e. to add the global warming CMIP SST pattern to the present-day observed mean state. Several authors have used this strategy to assess the sensitivity of the tropical Pacific rainfall response to CMIP mean state biases (Power et al., 2013; Widlansky et al., 2013; Chung et al., 2014; Dutheil et al., 2018). These studies demonstrate that the increase in equatorial Pacific rainfall variability in response to climate change is similar to that found in the CMIP ensemble projection but that the reduction in the cold-tongue bias further enhances the eastward shift in the location of main ENSO-related anomalies in convection.

It must however be mentioned that, while this bias correction approach is likely to improve the reliability of future projection, atmosphere-only present-day simulations still exhibit significant biases in their representation of the atmospheric response to ENSO (e.g., Zhang and Sun 2014; Ferret et al., 2017; Tang and Yu, 2018), which may still impair the reliability of the projected changes. Another dynamical approach is to use a flux correction strategy directly in coupled models to reduce present-day mean-state bias. By applying such a strategy, Cai et al. (2014)

suggested that the projected frequency increase in extreme El Niño events derived from CMIP model analyses should be even larger when correcting for model biases. However, minimizing mean-state biases through flux adjustment may not necessarily remove important biases in the dominant ENSO feedbacks and uncertainties in ENSO projections (Neelin & Dijkstra, 1995; Ferret & Collins; 2016).

Given ENSO is influenced by variability outside the tropical Pacific Ocean (Chapter 11), model biases in remote oceans would also be an important factor for ENSO simulation and projection. For instance, biases in Indian Ocean mean state and variability can affect the amplitude and frequency of simulated ENSO (Yu et al., 2009; Santoso et al., 2012). Further, recent studies have pointed out the underestimation of Pacific Trade Winds acceleration during the early 21st Century global warming hiatus period by climate models (e.g., Kociuba & Power, 2015) appears to be linked to biases in the Atlantic (Kajtar et al., 2018; McGregor et al., 2018), and underestimation of inter-basin relative warming (Luo et al., 2017). How this may impact on ENSO simulation remains to be investigated, and so does the ramifications for future projections of ENSO, in particular considering the potential that pan-tropical inter-basin interactions could be underestimated in climate models (Cai et al., 2019).

13.6. Summary and concluding remarks

From the discussions presented in this chapter based on various existing studies, there appears to be three factors that are key toward an understanding of how ENSO would change under global warming: 1) the tropical Pacific mean-state change; 2) changes in non-linear processes that interact with the mean climate; and 3) climate model fidelity. Most climate models project equatorially enhanced surface warming in the Pacific Ocean, with a weakening of the Walker Circulation (section 13.2; Fig. 13.1). This was found to lead to robust enhancement of ENSO-driven rainfall variability along the equatorial Pacific (section 13.4.1; Fig. 13.2), even though models do not tend to agree on changes in ENSO as measured using traditional SST metrics (section 13.3; Fig. 13.2).

On the other hand, considering only models that are able to simulate key nonlinear processes, such as rainfall response to eastern equatorial Pacific SSTs, eastward propagation of ENSO SST anomalies, large anomalous central Pacific cooling during a La Niña, it has led to a projection of increased frequency of extreme El Niño and extreme La Niña events (section 13.4). These models also project that extreme swing of extreme El Niño to extreme La Niña in the following year – a rare catastrophic sequence that occurred in 1997-1999 – would be more than double in frequency under increasing greenhouse-gas concentration in the atmosphere (Fig. 13.3). Finally, accounting for model ability to simulate ENSO flavors has led to a projection of enhanced Eastern Pacific ENSO variability (Fig. 13.4), stemming from more frequent occurrences of strong El Niño events (section 13.4.3). All these taken together point to a possibility of increased activity of extreme ENSO events in a warming climate. Nonetheless, there are still uncertainties surrounding these projections given persistent model biases (section 13.5). Even the best models are still not free of errors and biases.

Another influential factor to consider is internal variability. ENSO potentially exhibits highly diverse behavior in the absence of external forcing, as demonstrated by millennial-long simulations (e.g., Wittenberg, 2009; Borlace et al., 2013). Multi-model averaging may not entirely remove internal variability (e.g., Frankcombe et al., 2015), but requiring large ensembles with individual models (e.g., Maher et al., 2018). Studies based on a climate model with a large ensemble has shown that the range of internal variability in ENSO amplitude is substantial and comparable to the projection uncertainty based on the CMIP5 multi models (Zheng et al., 2018). The way forward to study future ENSO changes is to utilize large ensemble members in a multi-model environment to account for both differences in model physics and natural variability. In addition, the impact of the background warming on ENSO changes requires further investigation in this context (e.g., An & Choi, 2015; Zheng et al., 2018); particularly since the interaction between ENSO and the mean climate, as well as the nature of decadal climate variability, are still subjects of active investigation (Chapter 8). How the annual cycle could change under global warming is also still an open question, which is highly relevant for understanding future ENSO changes (see Chapter 21 for discussions).

Nonetheless, despite the projection uncertainties, recent studies based on models, observations, and paleo-reconstructions have suggested that the Pacific climate and ENSO variability might already have been altered by anthropogenic forcing. For example, Wang et al. (2015) concluded that the warming since 1960 observed in the western tropical Pacific and in high quality surface temperature records from small island states in the west Pacific can be reproduced by climate models only if they include anthropogenic forcing. More recently, Power et al. (2017) showed that the overwhelming majority of CMIP5 models exhibit an increase in the frequency of disruption to tropical Pacific precipitation that ENSO causes (Fig. 13.5). The model results imply that the ENSO-driven rainfall disruption experienced in the real world in the late 20th Century could be due to increases in anthropogenic greenhouse forcing. This is consistent with paleoclimatic studies that have shown that ENSO-driven variability seen in paleo records had already increased in the late 20th Century (McGregor et al., 2013; Cobb et al., 2013; see Chapters 5, 21). The results of Power et al. (2017) further suggested that the risks would be elevated in the future, should the rate of global warming continues. In addition, the risk would be locked in for at least the rest of the 21st Century even if global warming is limited below 2°C under the Paris Agreement. This last result is consistent with Wang et al. (2017) who found that the increased frequency of extreme El Niño would continue for about a century upon stabilization of global warming at 1.5°C, although the risk associated with extreme La Niña would be averted. Future changes in ENSO behavior are expected to impact on global rainfall, tropical cyclones, marine ecosystems, fisheries and the global carbon cycle (Chapters 16-20) via atmospheric and oceanic teleconnections (Chapters 14, 15).

To sum up, latest research has suggested that the response of ENSO to greenhouse forcing may manifest in more frequent stronger ENSO events. Given the large impact of ENSO on society, economy, and the environment, this result has important ramifications for risk management in a warming world. There are uncertainties associated with the projections due to model biases. However, preliminary approaches in bias correction and/or consideration as discussed above have indicated a possibility that the risk could have been underestimated. While we wait for improved models for more reliable projections, it is also important to sustain and enhance observations and paleo-reconstruction capabilities.

Acknowledgments

We thank two anonymous reviewers for their constructive feedback. W.C. is supported by National Key R&D Program of China (2018YFA0605700). L.W. is supported by National Natural Science Foundation of China (NSFC). W.C., G.W., and A.S. are supported by CSHOR and the Earth System and Climate Change Hub of the Australian Government's National Environment Science Program (NESP). CSHOR is a joint research Centre for

Southern Hemisphere Oceans Research between QNLM and CSIRO. S. P. is supported by NESP.

References

An, S. I. (2011). Atmospheric responses of Gill-type and Lindzen–Nigam models to global warming. *Journal of Climate*, 24(23), 6165-6173.

An, S.-I., & Choi, J. (2015). Why the twenty-first century tropical Pacific trend pattern cannot significantly influence ENSO amplitude? *Climate Dynamics*, 44, 133–146.

An, S.-I. & Jin, F.-F. (2004). Nonlinearity and asymmetry of ENSO. *Journal of Climate*, 17, 2399–2412.

An, S.-I., Kim, J.-W., Im, S.-H., Kim, B.-M., & Park, J.-H. (2012). Recent and future sea surface temperature trends in tropical Pacific warm pool and cold tongue regions. *Climate Dynamics*, 39, 1373–1383.

Bayr, T., Latif, M., Dommenget, D., Wengel, C., Harlaß, J., & Park, W. (2018). Mean-state dependence of ENSO atmospheric feedbacks in climate models. *Climate Dynamics*, *50*(9-10), 3171-3194.

Bellenger, H., Guilyardi, E., Leloup, J. Lengaigne, M. and Vialard, J. (2014). ENSO representation in climate models: from CMIP3 to CMIP5. *Climate Dynamics*, 42, 1999–2018.

Bonfils, C. J., Santer, B. D., Phillips, T. J., Marvel, K., Leung, L. R., Doutriaux, C., & Capotondi, A. (2015). Relative contributions of mean-state shifts and ENSO-driven variability to precipitation changes in a warming climate. *Journal of Climate*, *28*(24), 9997-10013.

Borlace, S., Cai, W., & Santoso, A. (2013). Multidecadal ENSO amplitude variability in a 1000-yr simulation of a coupled global climate model: Implications for observed ENSO variability. *Journal of Climate,* 26(23), 9399–9407. https://doi.org/10.1175/JCU-D-13-00281.1

Cai, W., Borlace, S., Lengaigne, M., van Rensch, P., Collins, M., Vecchi, G., et al. (2014). Increasing frequency of extreme El Niño events due to greenhouse warming. *Nature Climate Change*, *4*(2), 111–116. https://doi.org/10.1038/nclimate2100

Cai, W., Wang, G., Santoso, A., McPhaden, M. J., Wu, L., Jin, F.-F. et al. (2015a). Increased frequency of extreme La Niña events under greenhouse warming. *Nature Climate Change*, *5*(2), 132–137. https://doi.org/10.1038/nclimate2492

Cai, W., Santoso, A., Wang, G., Yeh, S.-W., An, S.-I., Cobb, K. M., et al. (2015b). ENSO and greenhouse warming. *Nature Climate Change*, *5*(9), 849–859.

Cai, W., Wang, G., Santoso, A., Lin, X., & Wu, L. (2017). Definition of extreme El Niño and its impact on projected increase in extreme El Niño frequency. *Geophysical Research Letters*, 44, doi:10.1002/2017GL075635.

Cai, W., et al. (2018). Increased variability of eastern Pacific El Niño under greenhouse warming. *Nature*, 564, 201-206.

Cai, W., Wu, L., et al. (2019). Pantropical climate interactions. *Science*, 363, doi:

10.1126/science.aav4236.

Cane, M. A.,Clement, A. C., Kaplan, A., Kushnir, Y., Pozdnyakov, D., Seager, R., et al. (1997). Twentieth-century sea surface temperature trends. *Science*, 275, 957-960.

Capotondi, A., Wittenberg, A. T., Newman, M., Di Lorenzo, E., Yu, J.-Y., Braconnot, P., Dewitte, B. (2015). Understanding ENSO diversity. *Bulletin of the American Meteorological Society*, 96(6), 921–938. https://doi.org/10.1175/BAMS-D-13-00117.1

Chadwick, R., Boutle, I., Martin, G. (2012). Spatial patterns of precipitation change in CMIP5: Why the rich don't get richer in the Tropics. *Journal of Climate*, doi:10.1175/JCLID-12-00543.1.

Chen, L., Li, T., Yu, Y., et al. (2017). A possible explanation for the divergent projection of ENSO amplitude change under global warming. *Climate Dynamics*, 49, 3799-3811.

Chung, C. T. Y., Power, S. B., Arblaster, J. M., Rashid, H. A. & Roff, G. L. (2014). Nonlinear precipitation response to El Niño and global warming in the Indo-Pacific. *Climate Dynamics*, 42, 1837–1856 (2014).

Chung, C. T. Y. & Power, S. B. (2014). Precipitation response to La Niña and global warming in the Indo-Pacific. *Climate Dynamics*, 43, 3293–3307.

Clapeyron, M. C. (1834). "Mémoire sur la puissance motrice de la chaleur". *Journal de l'École Polytechnique* (in French). 23, 153–190.

Clausius, R. (1850). "Ueber die bewegende Kraft der Wärme und die Gesetze, welche sich daraus für die Wärmelehre selbst ableiten lassen" *Annalen der Physik*, *155*(4): 500–524.

Clement, A. C., Seager, R., Cane, M. A., & Zebiak, S. E., (1996). An ocean dynamical thermostat. *Journal of Climate*, 9, 2190-2196.

Coats, S., & Karnauskas, K. B. (2017). Are simulated and observed twentieth century tropical pacific sea surface temperature trends significant relative to internal variability? *Geophysical Research Letters*, *44*(19), 9928-9937.

Cobb, K. M. et al. (2013). Highly Variable El Niño-Southern Oscillation Throughout the Holocene. *Science*, 339, 67-70, doi:10.1126/science.1228246.

Collins, M. (2000a). The E1-Niño Southern Oscillation in the second Hadley Centre coupled model and its response to greenhouse warming. *Journal of Climate*, 13, 1299-1312.

Collins, M. (2000b). Understanding uncertainties in the response of ENSO to greenhouse warming. *Geophysical Research Letters*, 27(21), 3509-3512.

Collins, M., et al. (2010). The impact of global warming on the tropical Pacific Ocean and El Niño. *Nature Geoscience*, 3, 391-397.

Collins, M., et al. (2011). Climate model errors, feedbacks and forcings: a comparison of perturbed physics and multi-model ensembles. *Climate Dynamics*, 36, 1737-1766.

Deser, C., Phillips, A.S., & Alexander, M. A. (2010). Twentieth century tropical sea surface temperature trends revisited. *Geophysical Research Letters*, 37, L10701.

DiNezio, P. N. et al. Climate response of the equatorial Pacific to global warming. *Journal of Climate*, 22, 4873–4892 (2009).

Dommenget, D., Bayr, T., & Frauen, C. (2013). Analysis of the non-linearity in the pattern and time evolution of El Niño Southern Oscillation. *Climate Dynamics*, *40*(11-12), 2825–2847. https://doi.org/10.1007/s00382-012-1475-0

Dutheil, C., et al. (2018). Impact of surface temperature biases on climate change projections of the South Pacific Convergence Zone. *Climate Dynamics*, in press.

England, M., et al. (2014). Recent intensification of wind-driven circulation in the Pacific and the ongoing warming hiatus. *Nature Climate Change*, 4, 222–227, doi:10.1038/nclimate2106.

Fedorov, A. V., & Philander, S. G. (2000). Is El Niño changing? *Science*, *288*(5473), 1997–2002. https://doi.org/10.1126/ science.288.5473.1997

Ferrett, S., Collins, M., & Ren, H. L. (2017). Understanding bias in the evaporative damping of El Niño–Southern Oscillation events in CMIP5 models. *Journal of Climate*, *30*(16), 6351-6370.

Ferrett, S., & Collins, M. (2016). ENSO feedbacks and their relationships with the mean state in a flux adjusted ensemble. *Climate Dynamics*, 1-20.

Frankcombe, L. M., England, M. H., Mann, M. E., & Steinman, B. A. (2015). Separating internal variability from the externally forced climate response. *Journal of Climate*, 28(20), 8184–8202. doi:10.1175/JCLI-D-15-0069.1

Graham, N. E., & Barnett, T. P. (1987). Sea surface temperature, surface wind divergence, and convection over tropical oceans. *Science*, 238, 657-659.

Guilyardi, E. (2006). El Niño mean state seasonal cycle interactions in a multi-model ensemble. *Climate Dynamics*, 26, 329–348.

Ham, Y.-G., & Kug, J.-S. (2012). How well do current climate models simulate two types of El Niño? *Climate Dynamics*, 39, 383-398.

Ham, Y.-G., & Kug, J.-S. (2014). ENSO phase-locking to the boreal winter in CMIP3 and CMIP5 models. *Climate Dyn.*, **43**, 305–318, doi:https://doi.org/10.1007/s00382-014-2064-1.

Ham, Y.-G., & Kug, J.-S. (2015). Improvement of ENSO simulation based on intermodel diversity, *Journal of Climate*, 28, 998–1015.

Ham Y.-G., & Kug, J.-S. (2016). ENSO amplitude changes due to greenhouse warming in CMIP5: Role of mean tropical precipitation in the twentieth century. *Geophysical Research Letters*, 43, doi: 10.1002/2015gl066864

Held, I. M., & Soden, B. J. (2006). Robust response of the hydrological cycle to global warming. *Journal of Climate*, 19, 5686-5699.

Hoerling, M. P., Kumar, A., & Zhong, M. (1997). El Niño, La Niña, and the nonlinearity of their teleconnections. *Journal of Climate*, 10, 1769–1786, https://doi.org/10.1175/1520-0442(1997)010<1769:ENOLNA>2.0.CO;2

Huang, P., & Xie, S. P. (2015). Mechanisms of change in ENSO-induced tropical Pacific rainfall variability in a warming climate. *Nature Geoscience*, *8*(12), 922.

Huang, P. (2016). Time-varying response of ENSO-induced tropical Pacific rainfall to global warming in CMIP5 models. Part I: Multimodel ensemble results. *Journal of Climate*, *29*(16), 5763-5778.

Huang, P., & Chen, D. (2017). Enlarged asymmetry of tropical Pacific rainfall anomalies induced by El Niño and La Niña under global warming. *Journal of Climate*, *30*(4), 1327-1343.

Jin, F.-F., Kim, S.-T., Bejarano, L. (2006). A coupled-stability index for ENSO. *Geophysical Research Letters*, doi.org/10.1029/2006GL027221.

Jin, F.-F., & Neelin, J. D. (1993). Modes of interannual tropical ocean-atmosphere interaction-a unified view. Part I: Numerical results. *Journal of the Atmospheric Sciences*, 50(21), 3477–3503. https://doi.org/10.1175/1520-0469(1993)050%3C3477:MOITOI%3E2.0.CO;2

Johnson, N., & Xie, S.-P. (2010). Changes in the sea surface temperature threshold for tropical convection. *Nature Geoscience*, 3, 842-845.

Kajtar, J. B., Santoso, A., McGregor, S., &England, M. H. (2018). Model under-representation of decadal Pacific trade wind trends and its link to tropical Atlantic bias. *Climate Dynamics*, 50, 1471-1484.

Kang, I. ‐ S., & Kug, J. ‐ S. (2002). El Niño and La Niña sea surface temperature anomalies: Asymmetry characteristics associated with their wind stress anomalies, *J. Geophys. Res.*, 107(D19), 4372, doi:10.1029/2001JD000393.

Karamperidou, C., Jin, F.-F. & Conroy, J. L. (2017). The importance of ENSO nonlinearities in tropical Pacific response to external forcing. *Climate Dynamics*, 49, 2695–2704.

Karnauskas, K. B., Seager, R., Kaplan, A., Kushnir, Y. & Cane, M. A. (2009). Observed strengthening of the zonal sea surface temperature gradient across the equatorial Pacific Ocean. *Journal of Climate* 22, 4316–4321.

Kim, S.-T., & Jin, F.-F. (2011). An ENSO stability analysis. Part II: results from the twentieth and twenty-first century simulations of the CMIP3 models. *Climate Dynamics*, 36, 1609-1627.

Kim, S.-T., Cai, W., Jin, F.-F., Santoso, A., Wu, L., Guilyardi, E., & An, S.-I. (2014a). Response of El Niño sea surface temperature variability to greenhouse warming. *Nature Climate Change*, 4, 786-790.

Kim, S.-T., W. Cai, F.-F. Jin, and J.-Y. Yu (2014b). ENSO stability in coupled climate models and its association with mean state. *Climate Dynamics*, 42, 3313–3321, doi:https://doi.org/10.1007

Knutson, T. R., & Manabe, S. (1995). Time-mean response over the tropical Pacific to increased CO2 in a coupled ocean-atmosphere model. *Journal of Climate*, 8, 2181-2199.

Knutson, T. R., Manabe, S. & Gu, D. (1997). Simulated ENSO in a global coupled ocean-atmosphere model: multidecadal amplitude modulation and CO2 sensitivity. *Journal of Climate*, 10, 138-161.

Knutson, T.R. Sirutis, J.J. Garner, S.T. Vecchi, G.A. and Held, I.M. (2008). Simulated reduction in Atlantic hurricane frequency under twenty-first-century warming conditions. *Nature Geoscience*, *1*, 359–364.

Kociuba, G. & Power, S. B. (2015). Inability of CMIP5 models to simulate recent strengthening of the Walker Circulation: implications for projections. *Journal of Climate*, 28, 20-35, doi: 10.1175/JCLI-D-13-00752.1.

Kohyama, T., Hartmann, D.L. & Battisti, D. S. (2017). La Niña–like Mean-State Response to Global Warming and Potential Oceanic Roles. *Journal of Climate,* 30, 4207–4225,https://doi.org/10.1175/JCLI-D-16-0441.1

Kohyama, T., Hartmann, D. L., & Battisti, D. S. (2018). Weakening of nonlinear ENSO under global warming. *Geophysical Research Letters*, *45*(16), 8557-8567.

Kosaka, Y. & Xie, S. P. (2013). Recent global-warming hiatus tied to equatorial Pacific surface cooling. *Nature*, 50158 (7467), 403-407, doi:10.1038/nature12534.

Kug, J. S., Sooraj, K. P., Jin, F. F., Ham, Y. G., & Kim, D. (2011). A possible mechanism for El Niño-like warming in response to the future greenhouse warming. *International Journal of Climatology*, 31(10), 1567-1572.

Latif, M., & Keenlyside, N. (2009). El Niño/Southern Oscillation response to global warming. *Proceedings of the National Academy of Sciences*, 106, 20578-20583.

Lau, W. K. M., & Kim, K.-M. (2015). Robust Hadley Circulation changes and increasing global dryness due to CO2 warming from CMIP5 model projections. *PNAS*, 112(12), 3630-3635.

Lee, T., & McPhaden, M. J. (2010). Increasing intensity of El Niño in the central-equatorial Pacific. *Geophysical Research Letters*, 37, L14603. https://doi.org/10.1029/2010GL044007

L'Heureux, M. L., S. Lee, and B. Lyon, 2013: Recent multidecadal strengthening of the Walker circulation across the tropical Pacific. Nature Climate Change, 3, 571–576, doi:https://doi.org/10.1038/nclimate1840.

Li, G. Du, Y. Xu, H. and Ren, B. (2015). An Intermodel Approach to Identify the Source of Excessive Equatorial Pacific Cold Tongue in CMIP5 Models and Uncertainty in Observational Datasets. *Journal of Climate*, *28*, 7630–7640.

Li, G., Xie, S.-P., Du., Y., & Luo Y. (2016). Effects of excessive equatorial cold tongue bias on the projections of tropical Pacific climate change. Part I: the warming pattern in CMIP5 multi-model ensemble. *Climate Dynamics*, 47, 3817-3831.

Liu, Z. (1998). On the role of ocean in theresponse of tropical climatology to global warming: The west-east SST contrast. *Journal of Climate*, 11, 864-875.

Liu, Z., Vavrus, S., He, F., Wen, N., & Zhong, Y., (2005). Rethinking tropical ocean response to global warming: The enhanced equatorial warming. *Journal of Climate*, 18, 4684-4700.

Liu, F., Luo, Y., Lu. J., & Wan, X. (2017). Response of the tropical Pacific Ocean to El Niño versus global warming. *Climate Dynamics*, 48, 935-956.

Lu, J., Vecchi, G. A., & Reichler, T. (2007). Expansion of the Hadley cell under global warming, *Geophysical Research Letters*, 34, L06805, doi:10.1029/2006GL028443.

McCreary, J. P., & Lu, P. (994). Interaction between the subtropical and equatorial ocean circulations:

The subtropical cell. *Journal of Physical Oceanography*., 24, 466–497.

Luo, JJ., Wang, G., & Dommenget, D. (2018). May common model biases reduce CMIP5's ability to simulate the recent Pacific La Niña-like cooling? *Climate Dynamics*, 50, 1335. https://doi.org/10.1007/s00382-017-3688-8

Maher, N., Matei, D., Milinski, S., & Marotzke, J. (2018). ENSO change in climate projections: Forced response or internal variability? *Geophysical Research Letters*, 45, 11,390– 11,398. https://doi.org/10.1029/2018GL079764

McGregor, S., Timmermann, A., England, M. H., Timm, O. E., & Wittenberg, A. T. (2013). Inferred changes in El Niño-Southern Oscillation variance over the past six centuries. *Climate of the Past*, 9, 2269-2284, doi:10.5194/cp-9-2269-2013.

McGregor, S., Spence, P., Schwarzkopf, F. U., England, M. H., Santoso, A., Kessler, W., Timmermann, A., Boening, C. (2014). ENSO driven interhemispheric Pacific mass transports. *Journal of Geophysical Research (Oceans)*, 119, 6221-6237.

McGregor, S., et al. (2018). Model tropical Atlantic biases underpin diminished Pacific decadal variability. *Nature Climate Change*, 8, doi:10.1038/s41558-018-0163-4.

McPhaden, M. J., & Zhang, X. (2009). Asymmetry in zonal phase propagation of ENSO sea surface temperature anomalies. *Geophysical Research Letters*, 36, L13703, http://dx.doi.org/10.1029/2009GL038774.

Mechoso, C., et al. (1995). The Seasonal Cycle over the Tropical Pacific in Coupled Ocean–Atmosphere General Circulation Models. *Monthly Weather Review*, 123, 2825–2838.

Meehl, G. A., & Washington, W. M. (1996). El Niño-like climate change in a model with increased atmospheric CO2 concentrations. *Nature*, 382,56-60.

Meehl, G. A., Brantstator, G.W. & Washington, W. M. (1993). Tropical Pacific interannual variability and CO2 climate change. *Journal of Climate*, 6, 42-63.

Merryfield, W. J. (2006). Changes to ENSO under CO2 doubling in a multimodel ensemble. *Journal of Climate*, 19, 4009–4027.

Neelin, D. J., et al. (1998). ENSO theory. *Journal of Geophysical Research*, 103, 14261–14290.

Neelin, J. D. & Dijkstra, H.A. (1995). Ocean-Atmosphere Interaction and the Tropical Climatology. Part I: The Dangers of Flux Correction. *Journal of Climate*, 8, 1325–1342, https://doi.org/10.1175/1520-0442(1995)008<1325:OAIATT>2.0.CO;2

Newman, M., Alexander, M. A., Ault, T. R., Cobb, K. M., Deser, C., DiLorenzo, E., et al. (2016). The Pacific Decadal Oscillation, revisited. *Journal of Climate*, 29(12), 4399–4427. https://doi.org/10.1175/JCLI-D-15-0508.1

Philip, S. Y., & van Oldenborgh, G. J. (2006). Shifts in ENSO coupling processes under global warming. *Geophysical Research Letters*, 33, L11704. doi: 10.1029/2006GL026196.

Philip, S. Y., & van Oldenborgh, G. J. (2009). Significant atmospheric nonlinearities in the ENSO cycle. *Journal of Climate*, 22, 4014-4028.

Power, S. B., & Delage, F. P. (2018). El Niño–Southern Oscillation and Associated Climatic Conditions around the World during the Latter Half of the Twenty-First Century. *Journal of Climate*, 31, 6189–6207, https://doi.org/10.1175/JCLI-D-18-0138.1

Power, S. B., & Kociuba, G. (2011a). What caused the observed twentieth century weakening of the Walker Circulation? *Journal of Climate*, 24, 6501-6514.

Power, S. B., & Kociuba, G. (2011b). Impact of global warming on the SOI. *Climate Dynamics*, 37, 1745-1754, doi: 10.1007/s00382-010-0951-7.

Power, S. B., & Colman, R. (2006). Multi-year predictability in a coupled general circulation model. *Climate Dynamics*, 26, 247-272.

Power, S. B., Delage, F., Chung, C., Kociuba, G., & Keay, K. (2013). Robust twenty-first century projections of El Niño and related precipitation variability, *Nature*, 502, 541-545, doi:10.1038/nature12580.

Power, S., Folland, C., Colman, A., & Mehta, V. (1999). Inter-decadal modulation of the impact of ENSO on Australia. *Climate Dynamics*, 15, 319-324.

Power, S., Haylock, M., Colman, R., & Wang, X. (2006). The predictability of interdecadal changes in ENSO and ENSO teleconnections. *Journal of Climate*, 8, 2161-2180.

Power, S. B., et al. (2017). Humans have already increased the risk of major disruptions to Pacific rainfall. *Nature Communications*, 8, 14368.

Rashid, H. A., Hirst, A. C., & Marsland, S. J. (2016). An atmospheric mechanism for ENSO amplitude changes under an abrupt quadrupling of CO2 concentration in CMIP5 models. *Geophysical Research Letters*, 43, doi: 10.1002/2015gl066768.

Rodgers, K.B., Friederichs, P., & Latif, M. (2004). Tropical Pacific decadal variability and its relation to decadal modulations of ENSO. *J. Climate,* 17, 3761–3774,https://doi.org/10.1175/1520-0442(2004)017<3761:TPDVAI>2.0.CO;2

Santoso A., England, M. H., & Cai, W. (2012). Impact of Indo-Pacific feedback interactions on ENSO dynamics diagnosed using ensemble climate simulations. *Journal of Climate*, 25, 7743-7763.

Santoso, A., McGregor, S., Jin, F. F., Cai, W., England, M. H., An, S. I., McPhaden, M., & Guilyardi, E. (2013). Late-twentieth-century emergence of the El Niño propagation asymmetry and future projections. *Nature*, *504*(7478), 126.

Santoso, A., McPhaden, M. J., & Cai, W. (2017). The defining characteristics of ENSO extremes and the strong 2015/16 El Niño. *Reviews of Geophysics*, doi:10.1002/2017RG000560.

Schneider, E. K. (1977). Axially symmetric steady-state models of the basic state for instability and climate studies, Part II. Nonlinear calculations, *Journal of Atmospheric Science*, 34, 280–296.

Schott, F. A., J. P. McCreary, & G. C. Johnson (2004). Shallow overturning circulations of the tropical–subtropical oceans. *Earth's Climate: The Ocean–Atmosphere Interaction, Geophysical Monograph,* Vol. 147, Amer. Geophys. Union, 261–304.

Seager, R., & Murtugudde, R. (1997). Ocean dynamics, thermocline adjustment and regulation of tropical SST. *Journal of Climate*, 10, 521–534.

Seo, K.-H., D. M. W. Frierson, and J.-H. Son (2014). A mechanism for future changes in Hadley circulation strength in CMIP5 climate change simulations. *Geophysical Research Letters*, 40, 5251–5258, doi:10.1002/2014GL060868.

Solomon, A., & Newman, M. (2012). Reconciling disparate twentieth-century Indo-Pacific ocean temperature trends in the instrumental record. *Nature Climate Change*, 2, 691-699.

Stein, K., Schneider, N., Timmermann, A., & Jin, F.-F. (2010). Seasonal synchronization of ENSO events in a linear stochastic model. *Journal of Climate*, 23, 5629-5643.

Stevenson, S. L. (2012). Significant changes to ENSO strength and impacts in the twenty-first century: Results from CMIP5. *Geophysical Research Letters*, 39, L17703. doi:10.1029/2012GL052759

Sun, D.-Z., Zhang, T., Sun, Y., & Yu, Y. (2014). Rectification of El Niño–Southern Oscillation into climate anomalies of decadal and longer time scales: Results from forced ocean GCM experiments. *Journal of Climate*, *27*(7), 2545–2561. https://doi.org/10.1175/JCLID-13-00390.1

Takahashi, K., Montecinos, A., Goubanova, K., & Dewitte, B. (2011). ENSO regimes: Reinterpreting the canonical and Modoki El Niño. *Geophysical Research Letters*, 38, L10704. https://doi.org/10.1029/2011GL047364

Takahashi, K., & Dewitte, B. (2016). Strong and moderate nonlinear El Niño regimes. *Climate Dynamics*, 46, 1627-1645.

Tang, S. L., & Yu, Y. Q. (2018). Evaluation of the zonal wind stress response to SST in the CMIP5 AMIP simulations. *Atmospheric and Oceanic Science Letters*, *11*(2), 157-164.

Taschetto, A. S., Sen Gupta, A., Jourdain, N., Santoso, A., Ummenhofer, C. C., & England, M. H. (2014). Cold tongue and warm pool ENSO events in CMIP5: mean state and future projections. *Journal of Climate*, 27, 2861-2885.

Tett, S. (1995). Simulation of El Niño-Southern Oscillation-like variability in a global AOGCM and its response to CO2 increase. *Journal of Climate*, 8, 1473-1502.

Timmermann, A. (2003). Decadal ENSO amplitude modulations: A nonlinear paradigm. *Global and Planetary Change*, 37, 135-156.

Timmermann, A., Oberhuber, J., Bacher, A., Esch, M., Latif, M., & Roeckner, E. (1999). Increased E1-Niño frequency in a climate model forced by future greenhouse warming, *Nature*, 398, 694- 696.

Timmermann, A. (2001). Changes of ENSO stability due to greenhouse warming. Geophysical Research Letters, 28, 2016-2064.

Timmermann, A., et al. (2018). El Niño-Southern Oscillation complexity. *Nature*, 559, 535-545.

Tokinaga. H., Xie, S.-P., Deser, C., Kosaka, Y., & Okumura Y. M. (2012a). Slowdown of the Walker circulation driven by tropical Indo-Pacific warming. *Nature*, 491, 439-443.

Tokinaga, H., Xie, S.-P., Timmermann, A., McGregor, S., Ogata T., et al. (2012b). Regional patterns of tropical Indo-Pacific climate change: Evidence of the Walker circulation weakening. *Journal of Climate*, 25, 1689-1710.

van Oldenborgh, G. J., Philip, S. & Collins, M. (2005). El Niño in a changing climate: a multi-model study. *Ocean Sci.*, 2, 267–298.

Vecchi, G. A. et al. (2006). Weakening of tropical Pacific atmospheric circulation due to anthropogenic forcing. *Nature*, 441, 73–76.

Vecchi, G. A. & Soden, B. J. (2007). Global warming and the weakening of the tropical circulation. J. Climate 20, 4316–4340.

Walker, C. C., & Schneider, T. (2006). Eddy-influences on Hadley circulations: Simulations with an idealized GCM, *Journal of Atmospheric Science*, 63, 3333–3350.

Wallace, J.M., et al. (1998). On the structure and evolution of ENSO-related climate variability in the tropical Pacific: lessons from TOGA. *Journal of Geophysical Research*, 103, 14241–14259.

Wang, B., & An, S.-I. (2001). Why the properties of El Niño changed during the late 1970s. *Geophysical Research Letters*, 28, 3709-3712.

Wang, B., & An, S. (2002). A mechanism for decadal changes of ENSO behavior: Roles of background wind changes. *Climate Dynamics*, 18(6), 475–486. https://doi.org/10.1007/s00382-001-0189-5

Wang, G., Power, S. B., & McGree, S. (2015). Unambiguous warming in the western tropical Pacific primarily caused by anthropogenic forcing. *International Journal of Climatology*, 36, 933-944, doi: 10.1002/joc.4395.

Wang, G., Cai, W., Gan, B., Wu, L., Santoso, A., Lin, X., Chen, Z., & McPhaden, M. (2017). Continued increase of extreme El Niño frequency long after 1.5C warming stabilization. *Nature Climate Change*, 7, 568-572.

Watanabe, M., et al. (2012). Uncertainty in the ENSO amplitude change from the past to the future. *Geophysical Research Letters*, 39, L20703.

Watanabe, M., Kamae, Y., & Kimoto, M. (2014). Robust increase of the equatorial Pacific rainfall and its variability in a warmed climate. *Geophysical Research Letters*, *41*(9), 3227-3232.

Widlansky, M. J., Timmermann, A., Stein, K., McGregor, S., Schneider, N., England, M.H., Lengaigne, M., & Cai, W. (2013). Changes in South Pacific rainfall bands in a warming climate. *Nature Climate Change*, *3*, 417–423.

Wittenberg, A. T. (2009). Are historical records sufficient to constrain ENSO simulations? *Geophysical Research Letters*, 36, L12702. https://doi. org/10.1029/2009GL038710

Xie, S.-P., et al. (2010). Global warming pattern formation: Sea surface temperature and rainfall. *Journal of Climate*, 23, 966-986.

Yeh, S.-W., & Kirtman, B. (2007). ENSO amplitude changes due to climate change projections in different coupled models. *Journal of Climate*, 20, 203-217.

Yeh, S.-W., et al. (2009). El Niño in a changing climate, *Nature*, 461, 511–514, doi:10.1038/nature08316

Yeh, S.-W., Kirtman, B. P., Kug, J.-S., Park, W., & Latif, M. (2011). Natural variability of the central Pacific El Niño event on multi-centennial timescales. *Geophysical Research Letters*, 38, L02704, doi:10.1029/2010GL045886.

Ying, J., Huang, P., Lian, T., & Tan, H. (2018). Understanding the effect of an excessive cold tongue bias on projecting the tropical Pacific SST warming pattern in CMIP5 models. *Climate Dynamics*, https://doi.org/10.1007/s00382-018-4219-y

Yu, J.-Y., Sun, F., & Kao, H.-Y. (2009). Contributions of Indian Ocean and monsoon biases to the excessive biennial ENSO in CCSM3. *Journal of Climate*, 22, 1850–1858.

Zhang, M. & Song, H. Evidence of deceleration of atmospheric vertical overturning circulation over the tropical Pacific. *Geophysical Research Letters*, 33, L12701 (2006).

Zhang, T., & Sun, D. Z. (2014). ENSO asymmetry in CMIP5 models. *Journal of Climate*, *27*(11), 4070-4093.

Zheng, X. T., Xie, S. P., Lv, L. H., & Zhou, Z. Q. (2016). Intermodel uncertainty in ENSO amplitude change tied to Pacific Ocean warming pattern. *Journal of Climate*, *29*(20), 7265-7279.

Zheng, X. ‐ T., Hui, C., & Yeh, S. ‐ W. (2018). Response of ENSO amplitude to global warming in CESM large ensemble: Uncertainty due to internal variability. Climate Dynamics, 50, 4019. doi:10.1007/s00382-017-3859-7

Zhou, Z.-Q., S.-P. Xie, X.-T. Zheng, Q. Liu, and H. Wang, 2014: Global warming–induced changes in El Niño teleconnections over the North Pacific and North America. *Journal of Climate*, 27, 9050–9064, https://doi.org/10.1175/JCLI-D-14-00254.1.

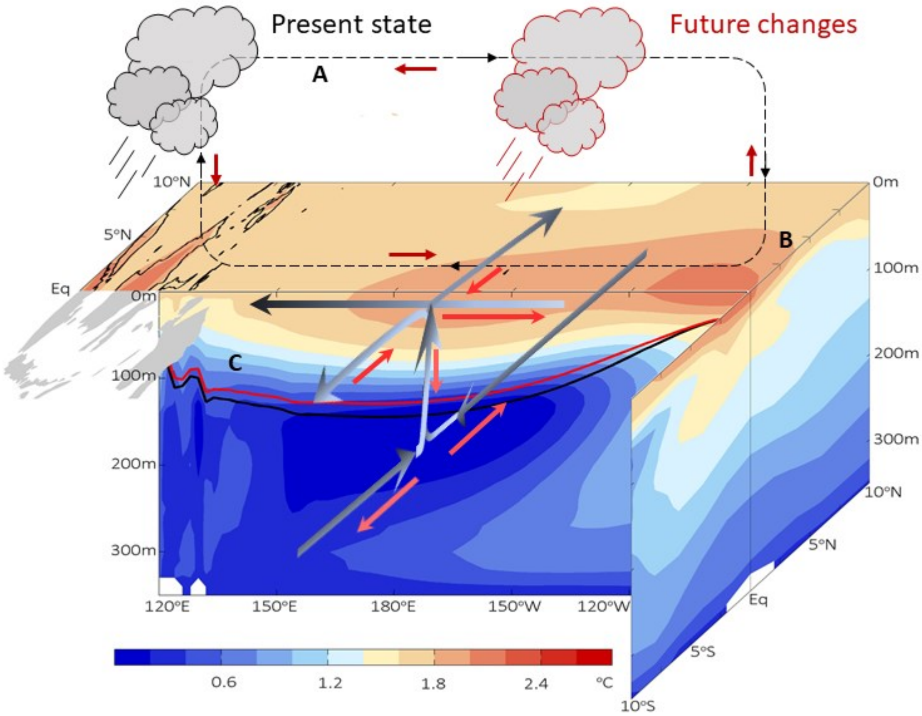

Figure 13.1: Schematic of tropical Pacific mean-state changes due to greenhouse forcing. Red arrows and red outlined clouds indicate greenhouse-induced changes. Present-day mean states are featured in black or gray (e.g., gray arrows indicate mean ocean circulations). Color shading denotes temperature change from present to future. (A) The Walker Circulation (dashed arrow) slows down, resulting in weaker westward flowing Trade Winds and ocean currents. (B) The equatorial region warms faster than off equator, with the eastern region and Maritime Continent warming faster than in the central Pacific. Atmospheric convection shifts towards eastern equatorial Pacific due to the reduced meridional and zonal temperature gradients. (C) The vertical ocean temperature gradient increases in response to increased radiative forcing at the surface, leading to shoaled thermocline. Present-day thermocline is indicated by the black curve in the ocean interior which shoals eastward, shallowing in the future as indicated by the red curve. Adapted from Cai et al. (2015b).

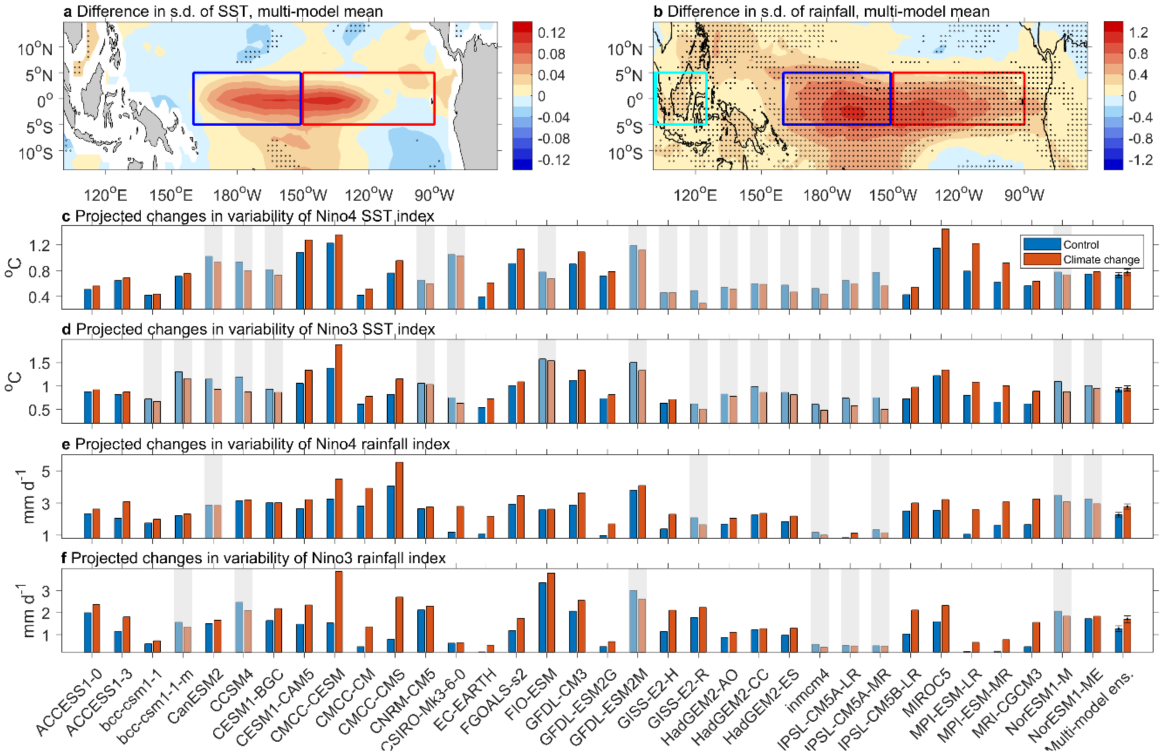

Figure 13.2: Greenhouse-warming induced change in sea surface temperature and precipitation variability over tropical Pacific. Results shown are based on CMIP5 outputs under historical and RCP8.5 emission scenario using 34 models, focusing on boreal winter (December-February average). **a**, Multi-model-mean change in SST standard deviation between future (2000-2099) and present-day (1900-1999). Niño4 (160°E-150°W, 5°S-5°N) and Niño3 (150°W-90°W, 5°S-5°N) regions are indicated by blue box and red box, respectively. Dotted areas mean that more than 70% of models (>~24 models) generate a change in phase with multi-model-mean value. **b**, As in **a**, but for rainfall (mm per day). Maritime Continent region (100°E -125°E, 5°S-5°N) used to construct zonal temperature gradient in Fig. 13.3b is indicated by cyan box. **c** and **d**, Projected changes in SST variability over Niño4 and Niño3 regions, respectively. Models that simulate a reduction are grayed out. Multi-model ensemble is also shown in both panels with error bars corresponding to the 95% confidence interval based on a bootstrap method. **e** and **f**, As in **c** and **d**, but for rainfall.

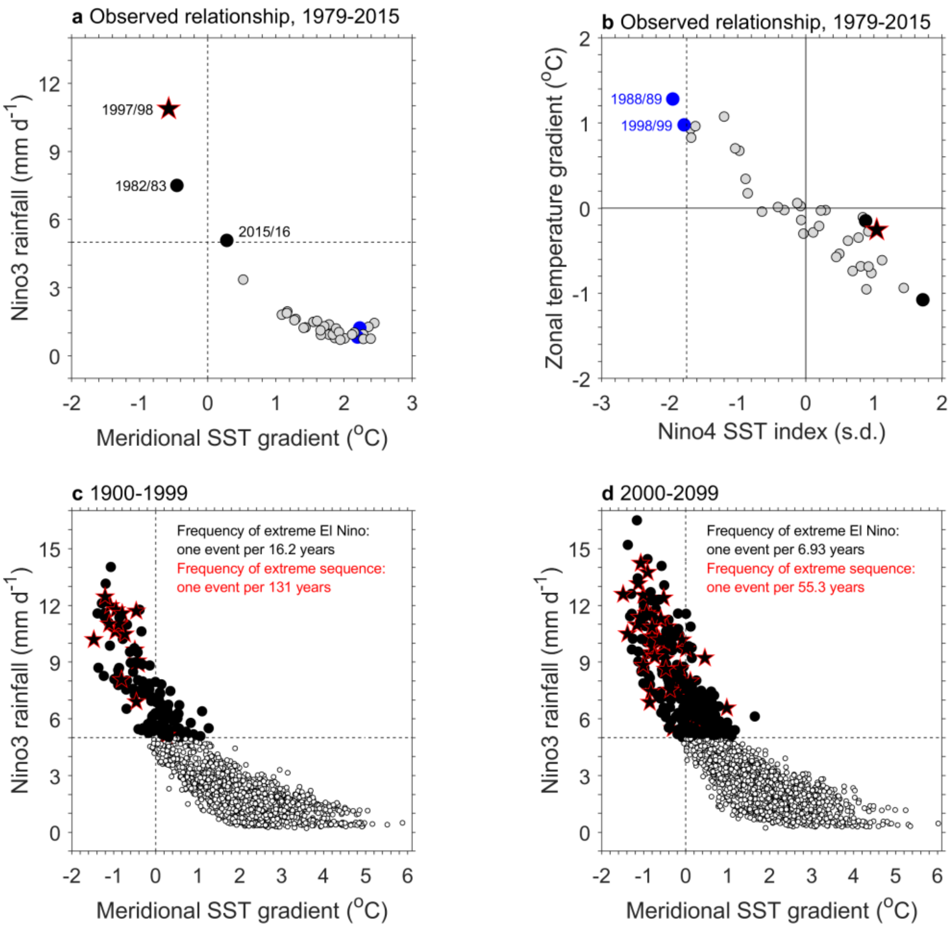

Figure 13.3: Observed climate extremes and greenhouse-warming induced changes. **a**, Observed relationship between Niño3 rainfall and meridional SST gradient (Cai et al 2014; 150°W-90°W, 5°N-10°N minus 150°W-90°W, 2.5°S-2.5°N). Black dots indicate extreme El Niño events, defined as when Niño3 rainfall is greater than 5 mm per day (marked by the horizontal line). Red star marks the 1997/98 event which was an extreme El Niño with concurrent eastward-propagating SST anomalies (Santoso et al., 2013) that was also followed by an extreme La Niña the following year (Cai et al., 2015b). **b**, Observed relationship between Niño4 SST and surface air temperature gradient between the Maritime Continent region (Fig. 13.2b) and Niño4 (Cai et al., 2015a). Blue dots indicate extreme La Niña events, defined as when Niño4 SST is negative and greater than 1.75 s.d. in amplitude. **c** and **d**, As in **a**, but using 21 selected CMIP5 models which can produce extreme El Niño events as in Cai et al. (2015b), under present-day (1900-1999) and future (2000-2099) respectively. Gray dots indicate events that are not extreme El Niño. As indicated within each panel, extreme El Niño occurs more frequently in future climate, from approximately one event per 16 years to one event per 7 years. A rare sequence of extreme events like in 1997-1998 is also projected to occur more often, from approximately one event per 131 years to one in 55 years.

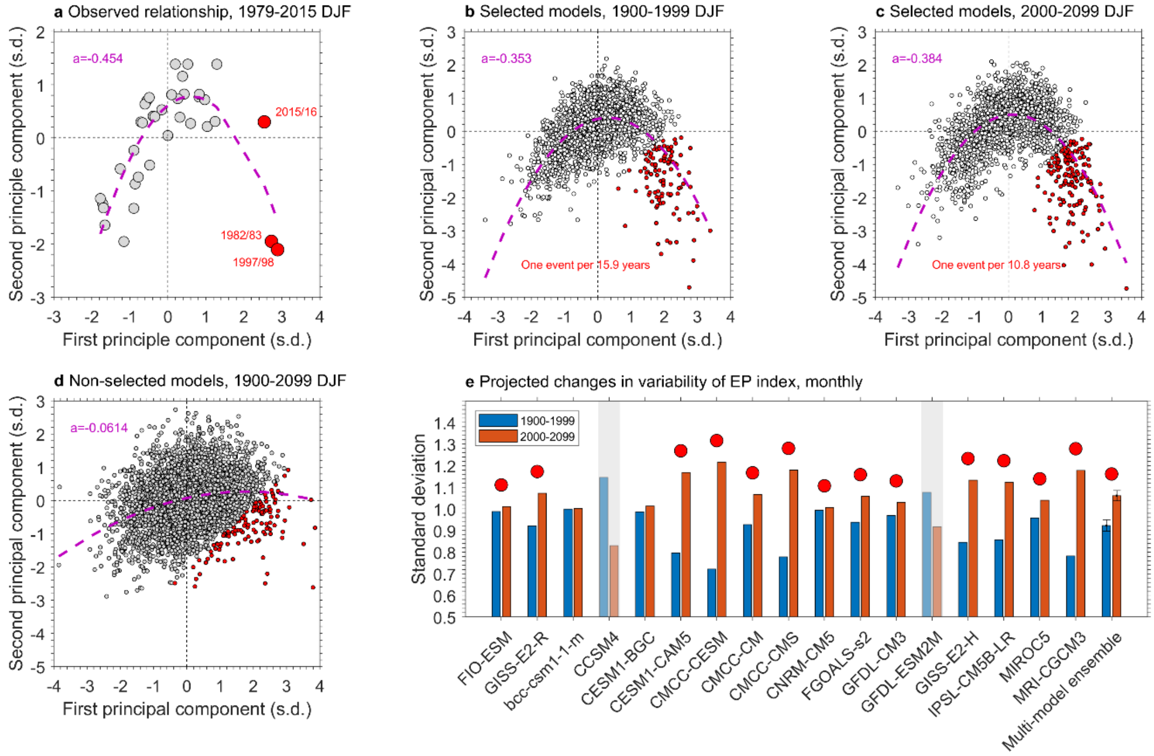

Figure 13.4: Eastern Pacific El Niño events defined by SST anomalies, and their projected changes under future climate**. a**, Observed relationship between the first two principal components using SST anomalies averaged over December-February ENSO peak phase. The EOF analysis for observations is applied to monthly SST anomalies referenced to their long-term monthly mean, over an equatorial domain (15° S–15° N, 140° E–80° W) to de-convolve spatio-temporal variability into orthogonal modes, each described by a principal spatial pattern and an associated principal component (PC) time series. The PC time series is scaled to have a standard deviation of one. The nonlinear relationship is determined by a quadratic fitting between PC1 and PC2: PC2(t)= α PC1(t)^2+βPC1(t)+ γ (Cai et al., 2018; Dommenget et al., 2013), as indicated by the purple curve. Red dots indicate strong EP El Niño events, defined by an E-index = $(PC1(t) - PC2(t))/\sqrt{2}$ (Takahashi et al., 2011) and when it is greater than 1.5 s.d. **b** and **c**, As in **a**, but using 17 models which are able to simulate at least half of the observed degree of nonlinearity measured by the parameter α (a in the panels), under present-day (1900-1999) and future (2000-2099), respectively (Cai et al., 2018). The EOF analysis for models is applied to monthly SST anomalies (from 1900 to 2099 forced with historical anthropogenic and natural forcings, and future greenhouse gases under the RCP8.5 scenario) which were firstly referenced to the monthly climatology of the first 100 years and then quadratically de-trended over the whole 200 years. Strong Eastern Pacific El Niño events are projected to occur more frequently under future climate, from approx. one in 16 years to one in 11 years. **d**, As in **a**, but using the remaining 17 models with weaker nonlinearity which is not sufficient to separate EP and CP El Niño. **e**, Projected changes in variability of the E-index using the 17 selected models. Blue and red bars indicate standard deviation of the E-index under present-day and future climate, respectively. Models simulating a decreased variability in E-index is greyed out. 15 out of 17 models produce an increased variability, in contrast to the poor inter-model agreement on the changes in Niño3 SST variability (Collins et al., 2010). Models with a red dot are able to project more occurrence of strong EP El Niño events. Increased E-index variability is associated with more occurrence of strong EP El Niño events in most models.

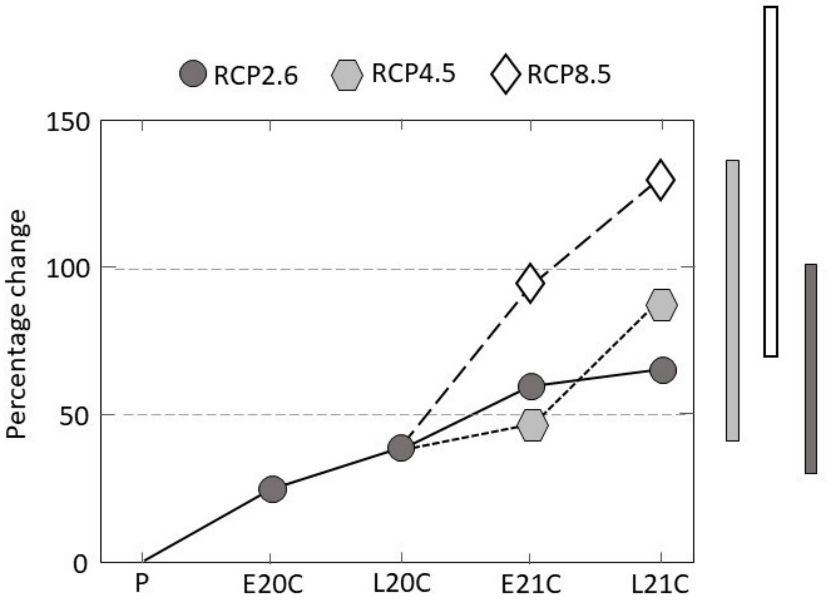

Figure 13.5: Percentage change in the frequency of major disruptions to precipitation over the tropical Pacific (140°E-240°E, 25°S-15°N) in the twentieth and twenty-first centuries, relative to the corresponding pre-industrial value of approximately (1.0/9.0 yr^{-1}). Results for the early 20^{th} century (E20C), late twentieth century (L20C), early 21^{st} century (E21C) and late 21^{st} century (L21C) are shown. The results are based on changes obtained from twenty CMIP5 models forced using pre-industrial control, historical forcing and three warming scenarios for the 21^{st} century: RCP2.6 (dark grey circle), RCP4.5 (light grey hexagon) and RCP8.5 (diamond). The lines and markers indicate percentage changes in the frequency of major disruption, relative to the pre-industrial value. The result is significant at the 90% level, under the assumption that models are independent. Adapted from Power et al. (2017).